공학석사학위논문

환형 막냉각에 대한 실험적 분석

Experimental investigation of circular array film cooling

2019년 2월

서울대학교 대학원

기계항공공학부

홍 준 영

환형 막냉각에 대한 실험적 분석

Experimental investigation of circular array film cooling

지도교수 황 원 태

이 논문을 공학석사 학위논문으로 제출함

2018년 10월

서울대학교 대학원

기계항공공학부

홍 준 영

홍준영의 공학석사 학위논문을 인준함

2018년 12월

위 원 장 _____최__해__천_____(인)

부위원장 _____황__원__태_____(인)

위 원 _____김__호__영_____(인)

Experimental investigation of circular array film cooling

Junyoung Hong
Department of Mechanical & Aerospace Engineering
Seoul National University

Abstract

In the present study, the effects of various factors on the effectiveness of circular array film cooling was experimentally investigated. The cooling effectiveness was obtained by non-dimensionalizing the measured temperature from an infrared camera. The experiment was carried out in a wind tunnel, and each design had a circular array of holes with different number and diameter. The area averaged effectiveness increased with coolant flow rate, and the design for 20 holes with 6 mm diameter provided the highest effectiveness. Regression analysis was conducted to investigate sensitivities for the main parameters, and the hole diameter was found to be the most sensitive parameter. In addition, based on the flow structure from CFD, we found that the flow from the upstream hole reattaches at the center of the surface and then mixes again with the main flow, together with the flow from the downstream holes.

Keyword: Circular array film cooling, infrared camera, cooling effectiveness
Student Number: 2017 – 27004

Table of Contents

List of Figures

List of Tables

Nomenclature

A	area
BR	blowing ratio
DR	density ratio,
L	streamwise length of cooling surface
$\dot{m}$	mass flow rate
R	radius of cooling surface
T	temperature
Tu	turbulence intensity
U	mean velocity
η	adiabatic effectiveness
ρ	density

Subscripts

∞	mainstream
aw	adiabatic wall
c	coolant

Chapter 1. Introduction

1.1. Research Background

The efficiency of a gas turbine increases with the combustion temperature, because it follows the Brayton cycle. Nowadays, by means of cooling and coating, the combustion temperature is over the melting point of the metal by hundreds of kelvins. To prevent economic loss due to blade failure, a blade monitoring system is desired. If an infrared camera is used, it is possible to monitor the blade temperature distribution non-destructively.

When using an infrared camera to monitor a rotating blade, an optical tube needs to be mounted on the turbine casing to transmit the optical information. The optical tube needs to be protected from the harsh gas turbine environment. Particularly, the optical window at the end of the optical tube must be thermally and optically protected, because it is directly exposed to the main hot gas and dust.

To protect the optical window, coolant flows along the outer edge of the tube and is ejected from multiple holes on the purge tip. Ejected coolant creates a film over the window surface, and cools and cleans the window. Because the array of holes is in a circular pattern, we have named this method "circular array film

cooling." Film cooling is a traditional external cooling method for gas turbine blades. However, the array of holes on a gas turbine blade is linear, which makes it different from the circular array film cooling used in this study. Much research has already been conducted for the traditional linear array film cooling. However, there have been no previous studies regarding circular array film cooling, which provides the motivation for this work.

1.2. Definition of flow and geometrical parameters

Performance of film cooling is influenced by various factors. Among them, special interest was given to flow parameters such as blowing ratio (*BR*) and density ratio (*DR*), or geometrical parameters such as hole shape, injection angle, compound angle, and the arrangement of holes. The blowing ratio is the mass flux ratio between the coolant and the main flow, which is defined in Equation 1.1:

$$BR = \frac{\rho_c U_c}{\rho_\infty U_\infty} = \frac{\dot{m}_c / A_c}{\dot{m}_\infty / A_\infty} \cdots\cdots\cdots\cdots Equation\ 1.1$$

DR is the density ratio between the coolant and the main flow, which is defined in Equation 1.2:

$$DR = \frac{\rho_c}{\rho_\infty} \cdots\cdots\cdots\cdots Equation\ 1.2$$

The important geometrical parameters in film cooling are the shape of the hole (Fig 1.1), the injection angle the hole makes with the main stream (Fig 1.2 a), the compound angle at which the cooling jets emerge (Fig 1.2 c), the hole pitch (Fig 1.3 a) and the number of rows (Fig 1.3 b). In the present study, in addition to the abovementioned parameters, the surface angle between the hole-punched surface and the main flow is also prescribed (Fig 1.2 b)

The goal for circular film cooling in this study is not only to lower the temperature of the window, but to also prevent dust accumulation. Both of these goals are related to how much the coolant mixes with the main flow. In order to quantify this mixing, we utilize the film cooling effectiveness, which is defined in Equation 1.3, where T_∞ is the main flow temperature, T_{aw} is the adiabatic wall temperature, and T_c is the coolant temperature.

$$\eta = \frac{T_\infty - T_{aw}}{T_\infty - T_c} \cdots\cdots\cdots\cdots Equation\ 1.3$$

1.3. Literature Survey

There have been many previous studies about film cooling. Many researchers have conducted experiments using a flat surface, which simplifies the actual airfoil geometry. This method is easier to replicate than an actual airfoil surface, and is useful for examining the effect of each parameter individually[1]. The results

found with this approach can be applied to real engine designs with slight corrections.

As mentioned above, flat surface modeling can examine the influence of various parameters belonging to flow condition and hole geometry. Among the parameters about the flow condition, BR and DR are considered as important parameters. As a result of experimenting with different *BR* when the other conditions were constant, the effectiveness decayed towards downstream and the rate was inversely proportional to *BR*[2−6]. *BR* is also a major variable on how the coolant separates from the surface. When *BR* is low, the coolant jet is fully attached to the surface. Conversely, if *BR* is high, the coolant jet is fully detached from the surface. When *BR* is in the middle, the coolant jet is detached from the surface and reattached at downstream. From the change in peak point and level, we can see that the separation characteristics of the flow affect the distribution of effectiveness[7, 8].

DR is the ratio of density as mentioned above. In a real gas turbine, *DR* = 2, but since this *DR* is difficult to make in an experimental facility, many experiments were performed in a low *DR*. When testing with a not real gas turbine *DR*, we can’ t match other parameters to real conditions[1]. Many studies have shown that *DR* does not have a significant impact on film effectiveness performance if other parameters are properly scaled[5, 6, 9]. In fact, according to experiments conducted at *BR* = 0.2, effectiveness

was essentially the same in the range of DR = 0.8 ~ 4.0. However, at higher BR, the lower the DR, the better the effectiveness is because the coolant has higher momentum and is separated from the surface[5]. Conversely, when DR was fixed to 1.2 or 1.8 and BR was 0.2 ~ 2.5 range, it was slightly better when DR was 1.8[6]. The above studies were performed with a flat surface model, but there was no significant difference when performed in air foil.

The geometry and configuration of the holes also have a large effect on the effectiveness of film cooling. For example, the film cooling effectiveness is improved by shaping the exit of the hole with an expansion so that the flow diffuses through the hole. Effectiveness with shaped hole was higher than cylindrical hole because deceleration occurred at exit and it makes coolant remain close to the wall. In this design called fan-shaped hole, when BR <4, since the separation due to the increase of BR is small, the effectiveness increases with increasing BR[10]. After it was found that the shaped hole was much better than cylindrical hole, experiments were carried out to investigate the effect of turbulence[11], compound angle[12, 13] and shape itself[14] on various shaped hole. Little different from changing the shape, there is also a tripod hole. This is a shape of a three-pronged hole in which a coolant jet exits through three holes with different compound angles[15].

Injection angle and compound angle also makes effect to film

cooling. At low *BR*, if other conditions were the same, the effectiveness decreased compared to 35° when the injection angle was 55° or 90°, because the coolant was separated from surface more[16]. At high *BR*, contrary, the effectiveness increased compared to 35° when the injection angle was 55° or 90° [6, 17]. When compound angle of hole is 60°, effectiveness is higher than 0° compound angle. This tendency appears stronger at higher *BR*. At a compound angle of 60°, the effectiveness is slightly increased at $BR = 0.25$, and nearly doubled at $BR = 0.98$, compared to compound angle of 0° [12, 13].

Arrangement of hole, spacing between hole and row, makes significant effect to film cooling performance, too. If the spacing between hole in a single row is large enough, the superposition prediction is well used because the coolant jets are independent of each other. Conversely, if the spacing is small, the coolant jet interferes with each other and creates continuous coverage, which increases effectiveness more than superposition predict[6, 17]. For $BR = 0.2$, superposition prediction is valid for two rows of holes. This is because coolant jet from each row do not interact with each other. For $BR \geq 0.5$, conversely, the two rows have higher effectiveness than superposition prediction[18]. There are also several studies about multiple rows with different compound angles or staggered arrangement[19, 20].

1.4. Research Objective

The present study is an investigation of circular array film cooling, where experiments were conducted for a few different designs which were downselected by CFD. Experiments were carried out at four flow levels for three designs, which had different diameter and number of holes. We conducted a sensitivity analysis on the key parameters, and investigated the flow structure using RANS CFD to corroborate the experimental results.

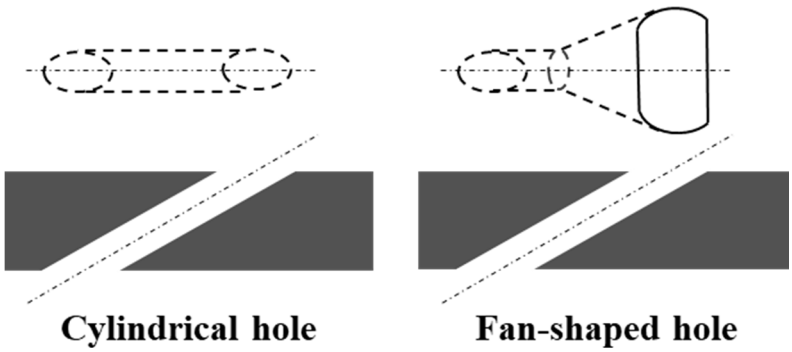

FIGURE 1.1 Schematics of hole shape. Left is for cylindrical hole and right is for fan-shaped hole.

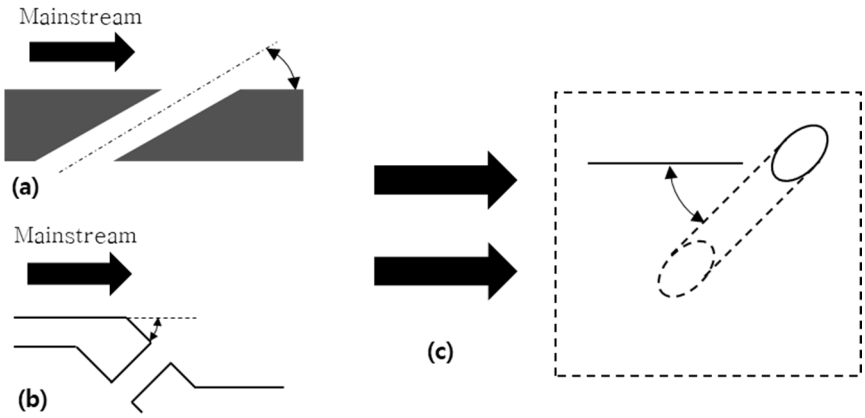

FIGURE 1.2 Schematics of (a) the injection angle, (b) the surface angle and (c) the compound angle. (a) and (b) is side view of coolant hole and (c) is top view of surface.

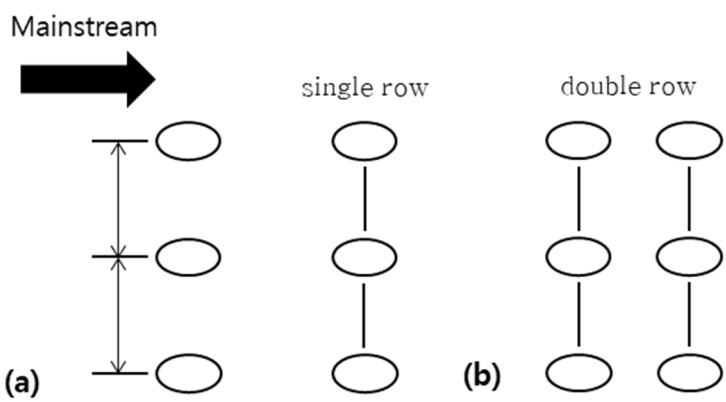

FIGURE 1.3 Schematics of (a) the hole pitch and (b) the number of rows for top view.

Chapter 2. Experimental method

2.1. Experimental setup

A diagram of the experimental setup is shown in figure 2.1. The experiments are performed in an open loop wind tunnel which has a test section of 600 x 300 x 1500mm^3(Width x Height x Length). The wind tunnel air flow velocity can be varied between 0 and 25 m/s, however, in this research we conducted experiments at 9 m/s only. The uniformity of the mean velocity and background Tu of the wind tunnel are both within 0.5% at 10m/s. The coordinate system is shown in figure 2.2 with the location of the purge tip. The upper surface of the purge tip is flush with the bottom of the test section.

The passageway of coolant flow beneath the purge tip is shown in figure 2.3. This toroidal passageway represents the actual flow path. At the top of the pipe, a threaded groove holds the purge tip. Three grids (4.23mm square mesh with round rod of 0.914mm diameter), are set under the purge tip to ensure uniform flow quality[21, 22]. As shown in figure 2.4, the purge tip is designed as a short cylindrical shape with a sharp inner tip for easy attachment and detachment. The sharp tip separates the coolant flow, allowing the flow to become developed within the toroidal passageway. The coolant is cooled by a heat exchanger using an ethylene glycol solution within a bath circulator (RW3-3035).

To minimize conduction error, the cooling surface is made by ABS which has a low conduction coefficient. The ease of coating high emissivity paint was one reason why this material was selected. The thickness of the ABS disk was 1mm, and insulation was fixed between the disk and lower component of the purge tip, as shown in Fig 2.4. The purge tip and cooling surface were painted with a high emissivity black paint (Aremco, 840-CM) to provide a high uniform emissivity, and also to prevent reflection.

Various measurement methods were used in the experiment. For the cooling surface, the 2-D temperature distribution was measured. For the main flow and coolant, temperature and pressure were measured at specific points. Furthermore, the velocity of the main flow and the mass flow rate of the coolant were respectively measured.

To obtain the 2-D temperature field of the cooling surface, a mid-wave infrared camera (A6753sc) is mounted above the test section. The camera viewed the purge tip and cooling surface through a sapphire window, which had a transmittance of 0.82 to mid-wave infrared radiation. Specifications of the camera are shown in Table 2.1.

For both main and coolant flow, k-type thermocouples were used to measure temperature. Transition joint probe thermocouple is fixed upstream of the test section. For coolant flow, the thermocouple is fixed at just before the hole, and the wires of the

thermocouple were inserted and welded at the center of the bolt to fix it at the wall. The location of the thermocouple is shown in Fig 2.3.

A pressure transducer (MSP-102) was used to measure the pressure of both flows. Measured points were upstream of the wind tunnel and just before the hole of the purge tip. At these specific points, a thin tube was connected between the pressure transducer and the measurement point in order to measure pressure[23].

To measure velocity of the main flow, a hot wire (TSI 8455) was used. The measured point was upstream of the wind tunnel. Because the hot-wire measures at a location near the thermocouple, each instrument was carefully positioned so that the two instruments do not interfere with each other.

The mass flow rate of coolant was measured by a flowmeter (KTVP-750). The flowmeter was installed under the wind tunnel. Sufficient length of piping was installed before and after the flowmeter for accurate measurements.

2.2. Experiment Procedure

To simplify the problem, we put constraints on some parameters. First, the hole angle and surface angle are fixed and perpendicular to make a cylindrical hole shape. Second, all flows use engineering air and maintain a constant temperature to keep the density ratio constant. Under these constraints, the experiment is

performed for 12 cases with four flow rates for three purge tip designs. In all designs, the injection angle and the surface angle equal 45 degrees. This is because the CFD indicated that a steeper angle provided higher cooling effectiveness, and this was the steepest angle that could be manufactured. In each design, the angles between the two adjacent holes were constant. Each design had different size and number of holes, as shown in table 2.2. The maximum flow rate was 310 L/min, and tested flow rates were about $\frac{1}{2}$, $\frac{2}{3}$, $\frac{5}{6}$, 1 of the maximum flow rate.

During the experiment, the position of the camera was fixed, and the purge tip was installed with one hole in the upstream direction as shown in Fig 2.5. Each parameter was measured as a time mean value. Each test was conducted after the coolant flows for a sufficient time for the setup to reach a thermally steady state.

After all experiments were completed, the IR thermography data is corrected for reflection and transmission[24]. Effectiveness is calculated using this corrected data.

2.3. Uncertainty

Uncertainties for all measurements were obtained. Repeatability was tested for all measurements, and bias was also obtained if possible. Reproducibility was checked on a daily basis. Bias was calculated as the difference between the time mean and the true value. Repeatability was calculated as shown in Equation 2.1. U_p is

repeatability and C_p is a constant depending on the degree of freedom. N is the number of samples. $\bar{p}$ is average of sample value and p_i is i_{th} sample value. When calculating repeatability, each sample is assumed to have an appropriate distribution[25].

$$U_p = C_p \sqrt{\frac{\sum_{i=1}^{N}(\bar{p} - p_i)^2}{N-1}} \cdots\cdots\cdots\cdots Equation\ 2.1$$

Since it is difficult to know the true value of the temperature in the actual experiments when measuring with an infrared camera, the uncertainty was obtained by setting the atmospheric temperature as the true value when neither the main flow or the coolant flow were flowing. The cooling surface was photographed at 1 Hz for 1 minute, and the 60 samples were assumed to follow the student−T distribution. The bias error was calculated by comparing with the atmospheric temperature (Fig 2.6 a). Repeatability was calculated for each pixel within the 2−D map (Fig 2.6 b). The area averaged values of bias and repeatability are 0.54C° and 0.06 C° respectively [26].

The two thermocouples were calibrated by a bath circulator (Fig 2.7). Uncertainty was determined for each measured temperature (Fig 2.8). The 600 samples were measured at 10 Hz for 1 minute. Uncertainty and error were calculated assuming a Gaussian distribution. Mean bias of thermocouple was −0.9 and

repeatability was 0.1 C°.

Uncertainty of flowmeter and hotwire were obtained in the same way. The samples were measured at 10Hz for 1 minute. Uncertainties were calculated assuming a Gaussian distribution. Repeatability of the flow meter was 5.9%, and repeatability of the hotwire was 1.1%

Uncertainty of parameters such as effectiveness and BR are obtained from the method shown in Equation 2.2. R is a parameter and x_1, x_2, ⋯, x_n are measurement parameter used to calculate R. U_R is uncertainty of R and U_{x_1}, U_{x_2}, ⋯, U_{x_n} are uncertainty of x_1, x_2, ⋯, x_n respectively.

$$R = f(x_1, x_2, \cdots, x_n)$$

$$U_R = \sqrt{(\frac{\partial R}{\partial x_1} U_{x_1})^2 + (\frac{\partial R}{\partial x_2} U_{x_2})^2 + \cdots + (\frac{\partial R}{\partial x_n} U_{x_n})^2} \cdots\cdots\cdots\cdots Equation\ 2.2$$

Equation of Effectiveness was shown in Equation 1.3. Area averaged uncertainty of effectiveness for all cases is shown in Fig 2.9. Furthermore, reproducibility of effectiveness is also included in Fig 2.9. The reproducibility was calculated by the difference between the values of the two data whose execution dates were different and the other conditions were the same.

Equation of *BR* was shown in Equation 1.1. In the same way as effectiveness, uncertainty of *BR* for all cases was calculated and

shown in Fig 2.10.

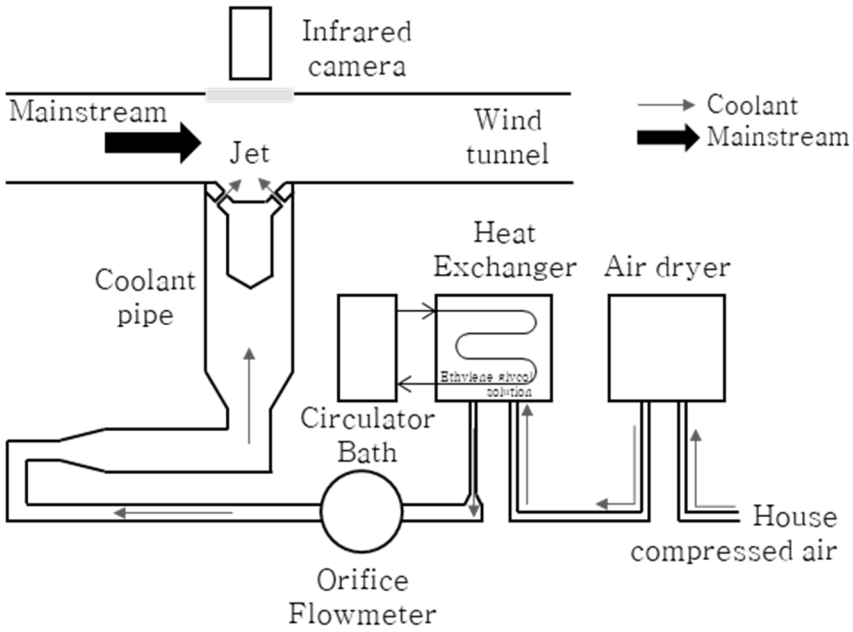

FIGURE 2.1 Diagram of experimental setup. Thin blue arrow is for coolant and thick black arrow is for mainstream

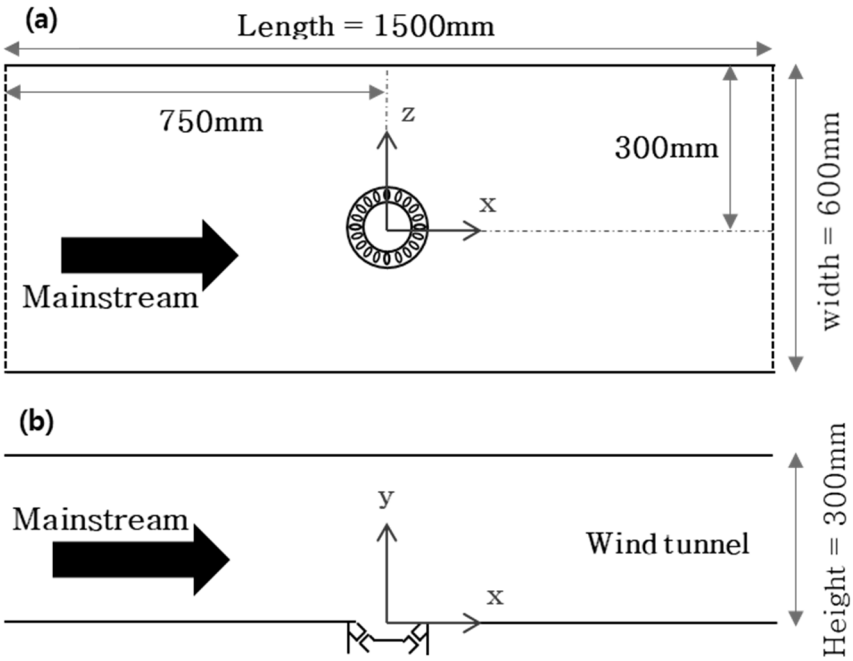

FIGURE 2.2 Coordinate system and location of purge tip (a) top view and (b) side view of test section. Purge tip is installed at the lateral center of the test section

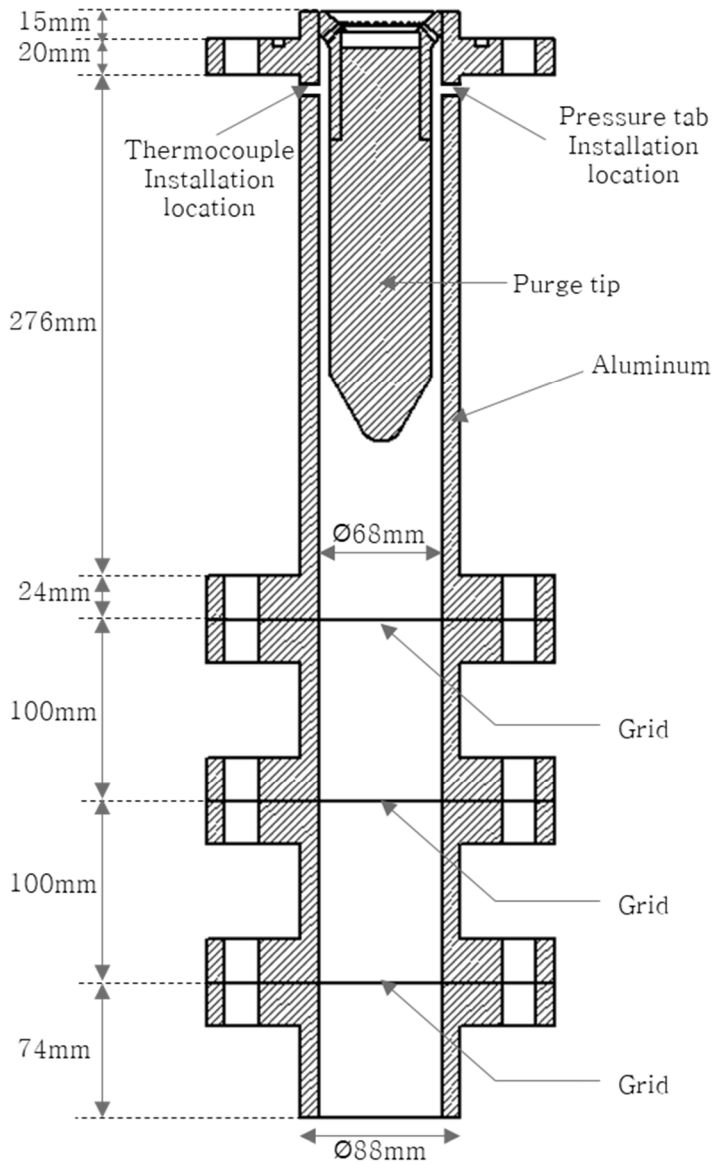

FIGURE 2.3 y−z plane cross section of coolant flow passageway. Circular passageway is below the purge tip and becomes a toroidal passage at the purge tip.

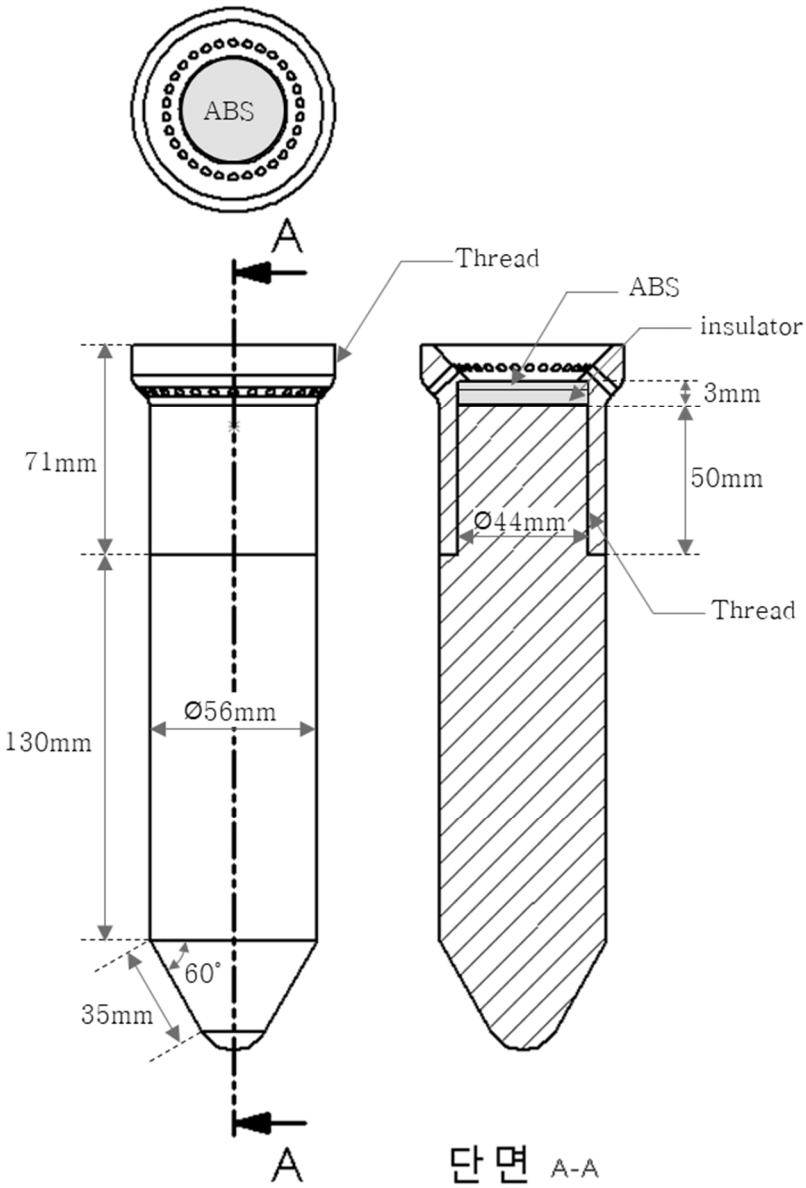

FIGURE 2.4 Structure of the purge tip. Top view, side view, and cross section.

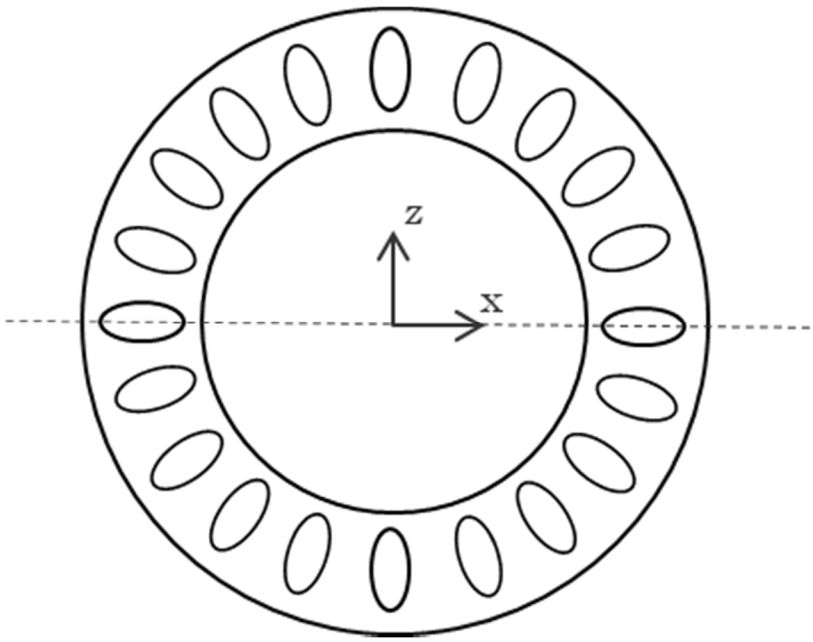

FIGURE 2.5 Top view of the installed purge tip

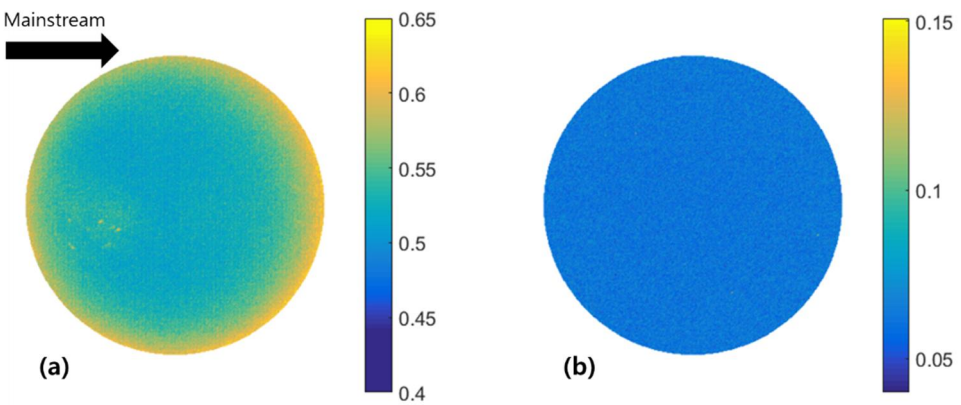

FIGURE 2.6 Uncertainty distribution of temperature(℃) measured by Infrared camera for (a) bias and (b) repeatability

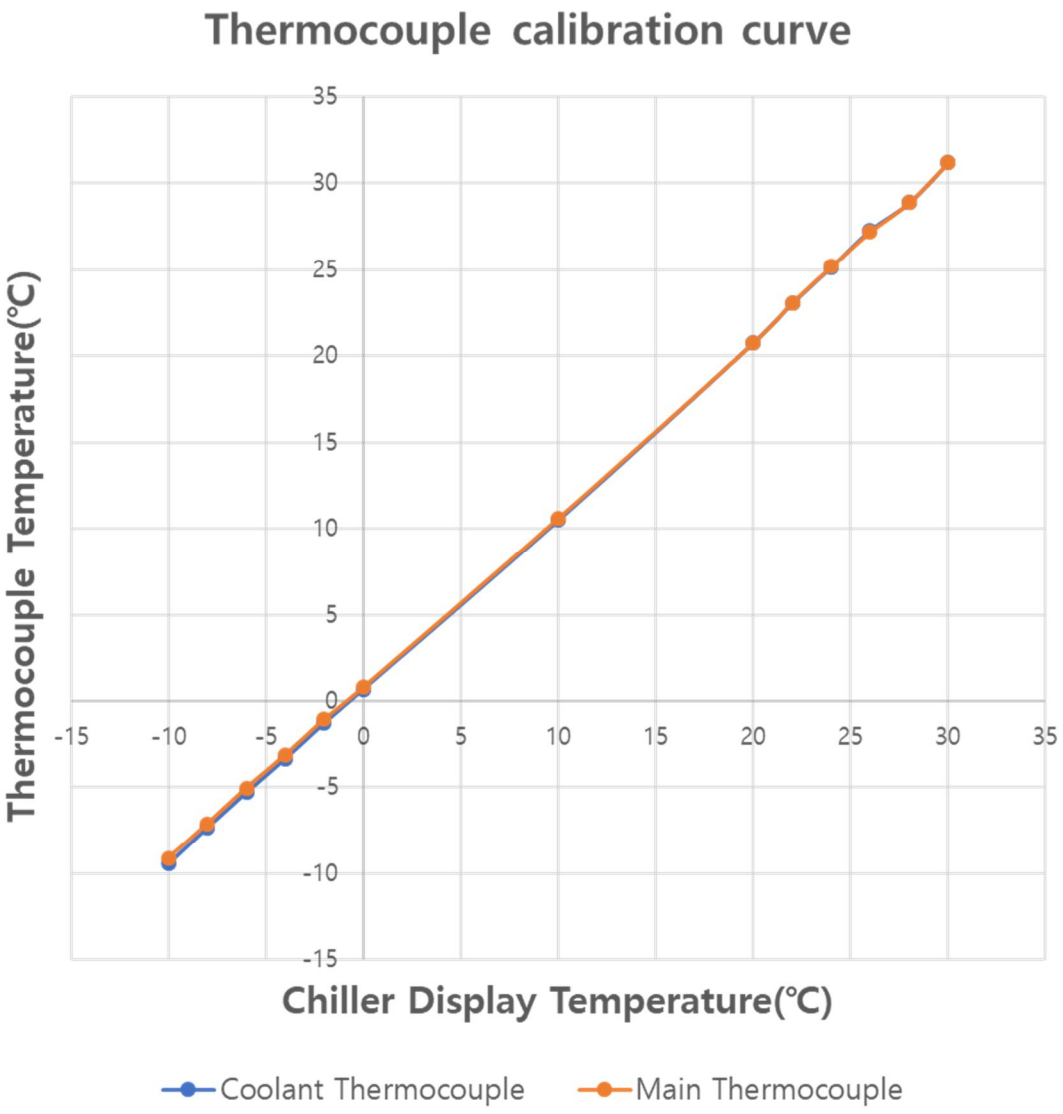

FIGURE 2.7 Calibration data of thermocouple. Blue line is for coolant thermocouple and orange line is for main thermocouple

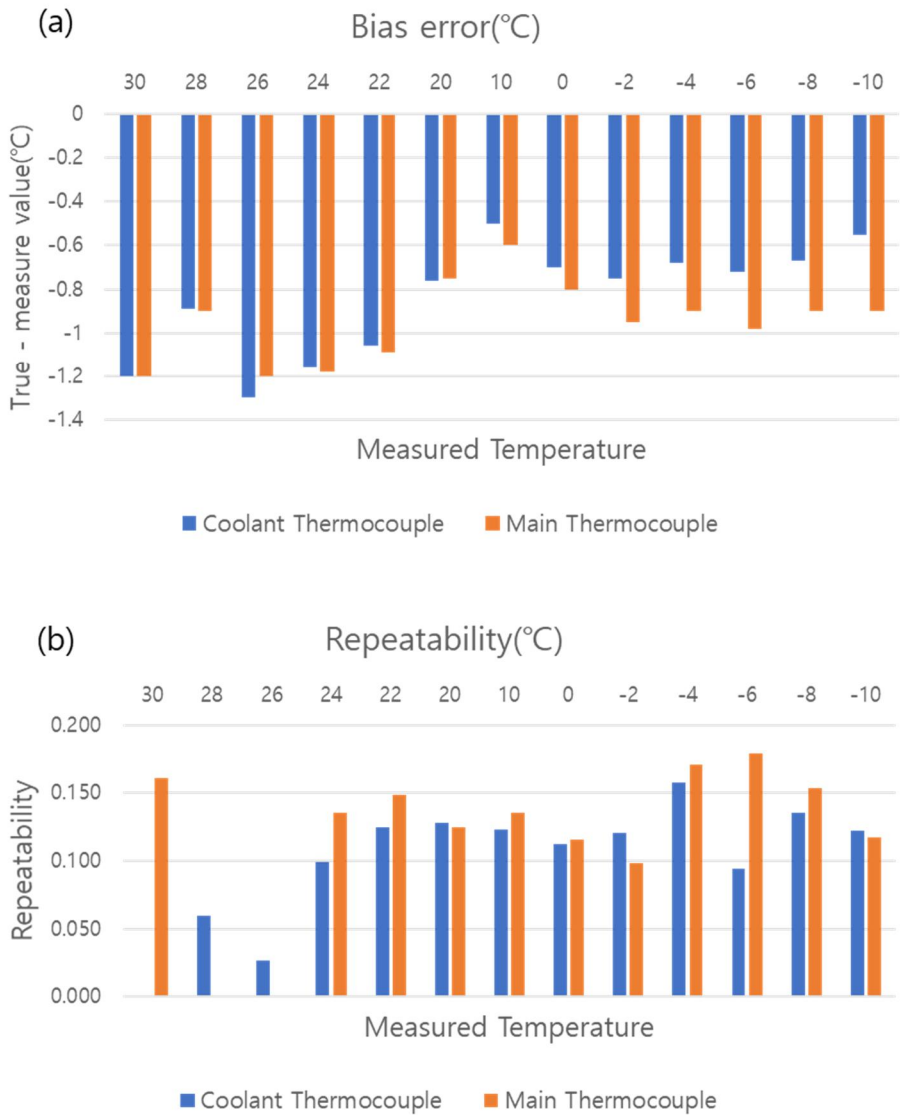

FIGURE 2.8 Uncertainty of thermocouple at various temperature for (a) bias and (b) repeatability. Blue bar is for coolant thermocouple and orange bar is for main thermocouple.

(a)

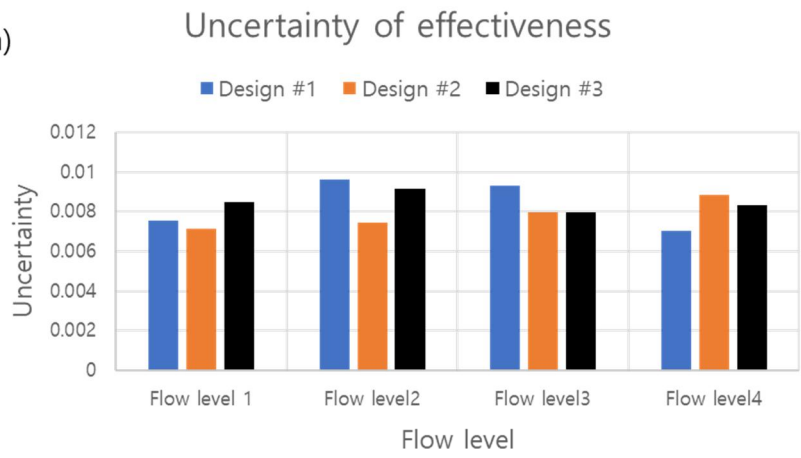

(b)

Design #1	1st	2nd	Absolute difference
FL4	0.8564	0.8582	0.0018
FL3	0.804	0.8169	0.0129
FL2	0.7075	0.7172	0.0097
FL1	0.6825	0.6545	0.028

FIGURE 2.9 (a)Area averaged uncertainty for all cases and (b)reproducibility of effectiveness for Design #1 case

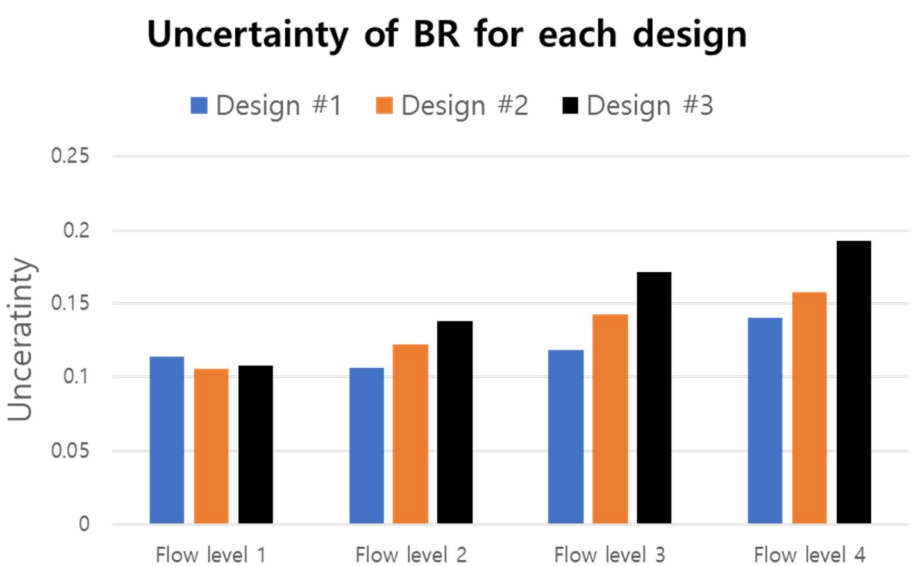

FIGURE 2.10 Uncertainty of Blowing Ratio for each design and flow level.

Model	FLIR A6750sc MWIR
Detector type	FLIR Indium Antimonide
Spectral Range	3 ~ 5um
Resolution	640 x 512
Dynamic Range	14 – bit
Integration time	480 ns to 687 sec

TABLE 2.1 Specification of mid wave infrared camera.

Design	#1	#2	#3
Hole diameter	3mm	4mm	6mm
The number of holes	30	30	20
Injection angle	45°		
Surface angle	45°		

TABLE 2.2 Design parameter of each purge tip design

Chapter 3. Experimental Results

3.1. Effectiveness distribution of cooling surface

From effectiveness of the cooling surface we know indirectly what part of the cooling is doing well or not. Fig 3.1 to 3.3 are 2-D distributions of the effectiveness for design #1, #2, and #3, respectively. The main flow is from left to right. Each figure consists of different flow level results performed for the same design. Some inhomogeneities in the distributions exist because the paint coating is not perfectly homogeneous. This problem is most pronounced for design #1.

According to Fig 3.1 ~ 3.3, the effectiveness scales with the mass flow rate. Fig 3.1 and 3.2 shows another trend, where effectiveness is high in the near-center area at all flow levels, and is lower towards the edge. It can also be seen that the upstream is less effective than the downstream at the edge. Additional analysis regarding this trend will be discussed again in Chapter 3.2 and 3.3.

Fig 3.4 shows the area averaged results, plotted against normalized flow level and *BR*. Fig 3.4 (a) shows that effectiveness scales with the normalized volume flow at all design. Also, design #3 is highest effective and design #1 is lowest effective at all flow level. Since *DR* is constant, *BR* is proportional to the flow level in

the same design. However, when the design is different, the overall width of the hole differs from design to design, resulting in differences of *BR* for each design at the same flow level.

3.2. Laterally averaged effectiveness

Laterally averaged cooling effectiveness is traditionally used in film-cooling research. The effectiveness is laterally averaged over each row normal to the streamwise direction of the cooling surface, as shown in Fig 3.5. Laterally averaged effectiveness proved to be a good indicator of the ultimate effect of the coolant [27].

Fig 3.6 to 3.9 are laterally averaged effectiveness for flow level 1~4. Each figure consists of results from different designs performed at the same flow level. The dotted line in the figures is a second order polynomial trend line for each data set. As shown in the figure, it fits well for most cases. As mentioned in Chapter 3.1, upstream is less effective than the downstream at the edge. Also, effectiveness is generally high at the center, and highest between x / L = 0.6 to 0.7. This is presumably due to the coolant flow, which exits the holes in a cone-like fashion. If there were no main flow, the cone-like coolant flow would make the effectiveness distribution be symmetrical. In this case, laterally average effectiveness would be highest in the center. But when the main flow exists, the cone-like coolant flow is pushed in the downstream direction. As the effectiveness distribution is pushed downstream,

the upstream region is less effective than downstream.

3.3. Half circle averaged effectiveness

Laterally averaged effectiveness is a good way to see how effectiveness changes in the streamwise direction, because usual film cooling studies use a linear hole array and a square downstream area. For circular array film cooling, a new concept of half circle averaged effectiveness is proposed. As shown in Fig 3.10, the area is divided into two semicircles, upstream and downstream, and the half circle averaged effectiveness is obtained for each.

Fig 3.11 to 3.14 show half circle averaged effectiveness for flow level 1~4. Each figure consists of results from different designs performed at the same flow level. The dotted line and dash dotted line of the figures is a second order polynomial trend line for each data set. As shown in the figure, it fits well for most cases. As mentioned in Chapter 3.1, effectiveness is generally high at the center and decreases smoothly toward the edge. In most cases, downstream value at the same r / R had higher results than the upstream value. Especially at r / R = 1, the downstream value in all cases was greater than the upstream value. In most cases, effectiveness is highest between r/R = 0.3~ 0.4 of downstream for each design. This is consistent with the results in Chapter 3.2. On the other hand, in the case of design #1, as the flow level increases, it does not fit well with the second-order polynomial trend line.

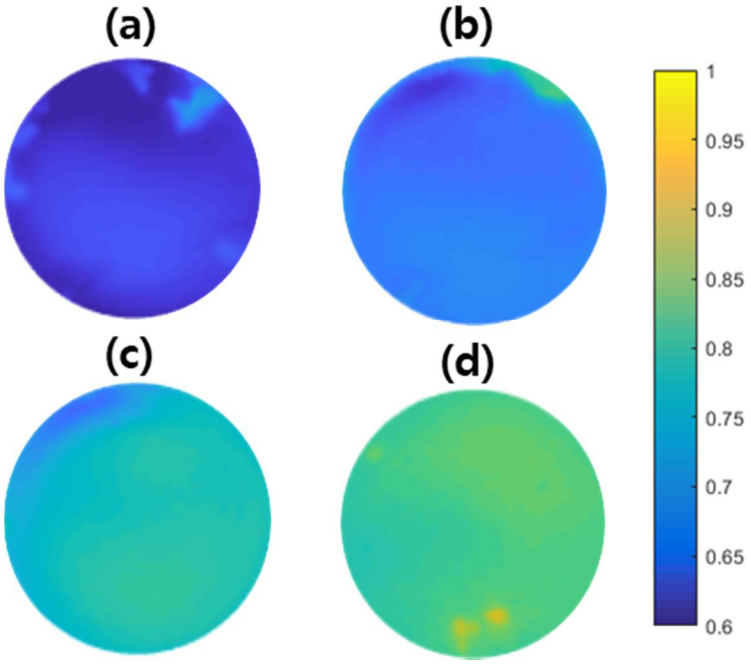

FIGURE 3.1 Effectiveness distribution of Design#1 for (a) Flow level 1, (b) Flow level 2, (c) Flow level 3 and (d) Flow level 4

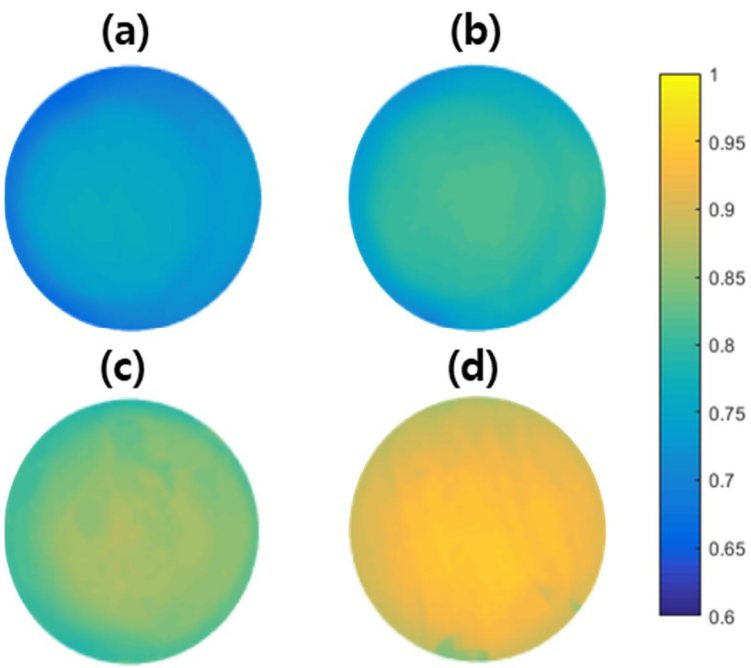

FIGURE 3.2 Effectiveness distribution of Design#2 for (a) Flow level 1, (b) Flow level 2, (c) Flow level 3 and (d) Flow level 4

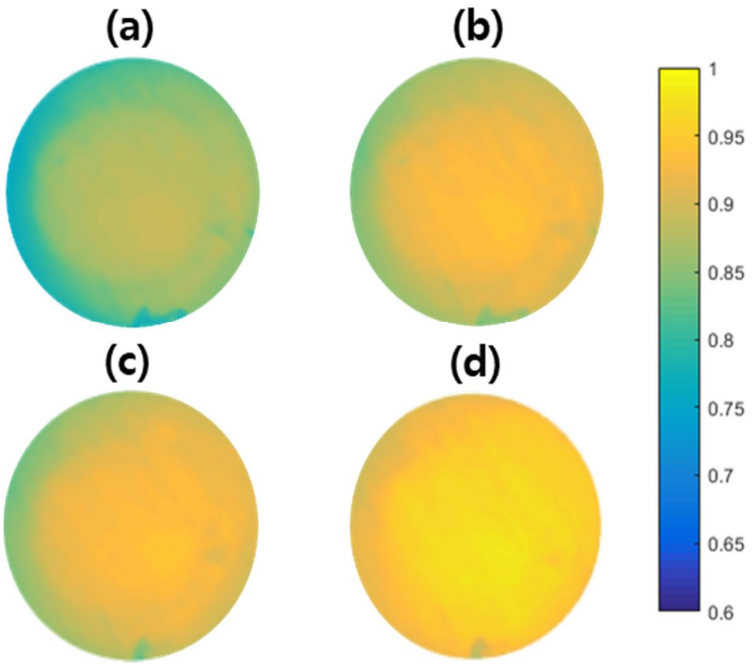

FIGURE 3.3 Effectiveness distribution of Design#3 for (a) Flow level 1, (b) Flow level 2, (c) Flow level 3 and (d) Flow level 4

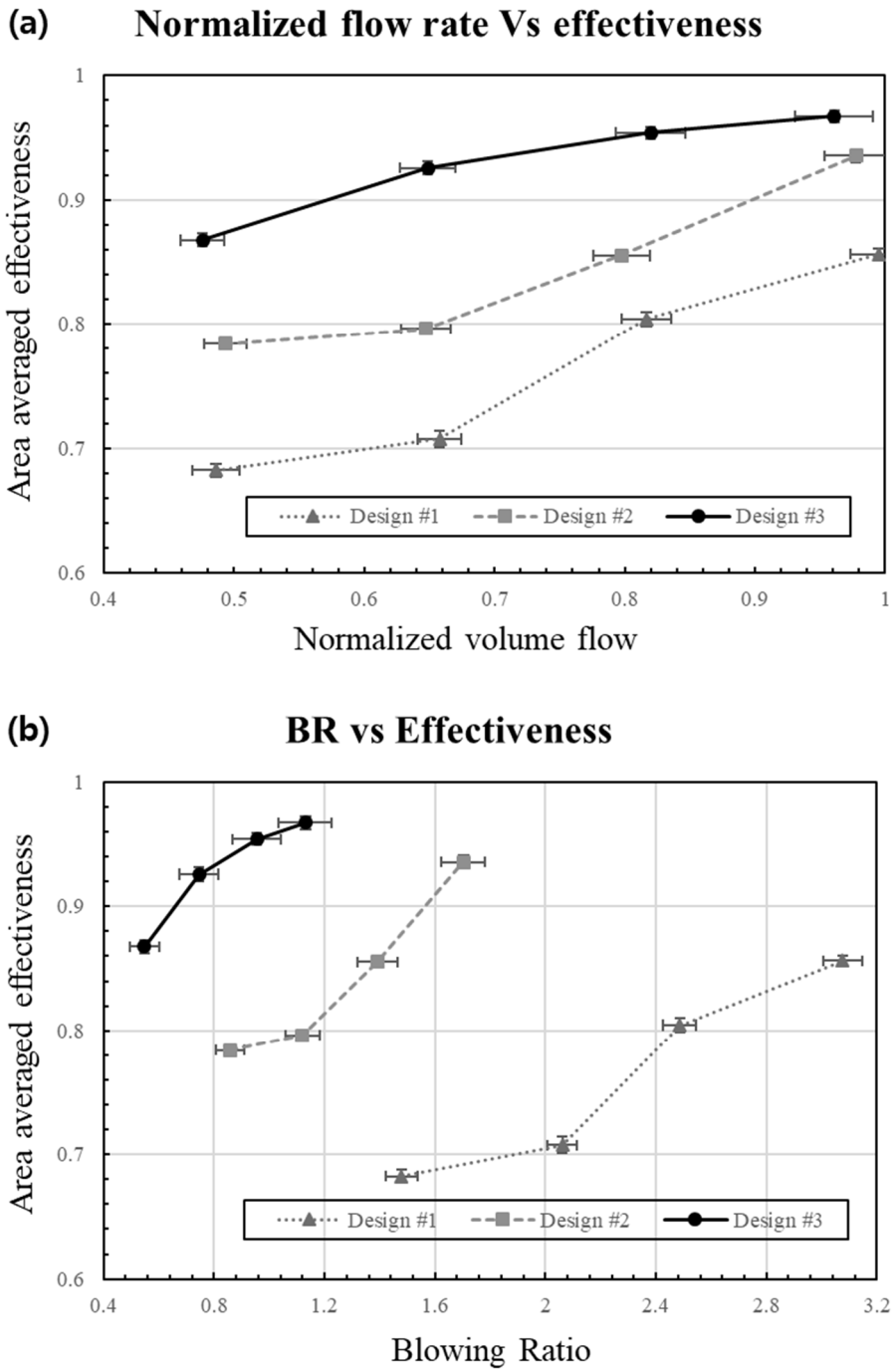

FIGURE 3.4 Area averaged effectiveness (a) vs Flow level and (b) vs BR

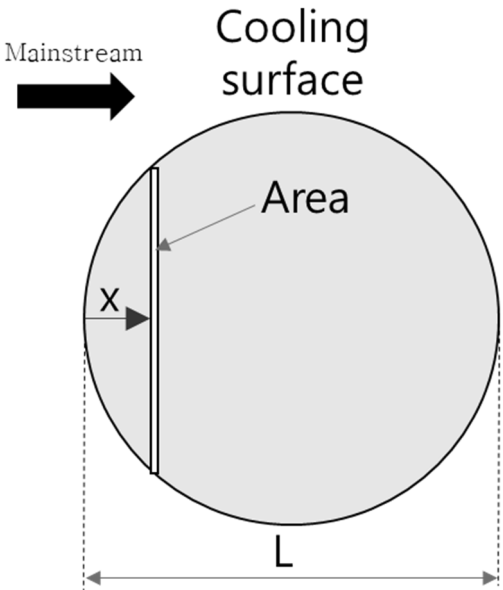

FIGURE 3.5 Schematic of laterally averaged effectiveness.

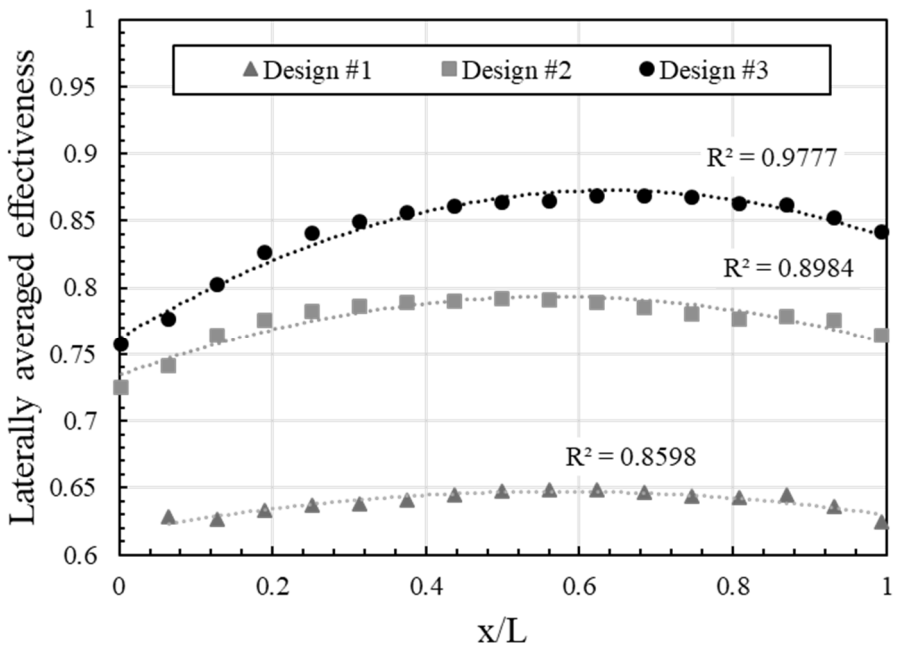

FIGURE 3.6 Laterally averaged effectiveness for Flow level 1. Dotted line is second order polynomial trend line for each data

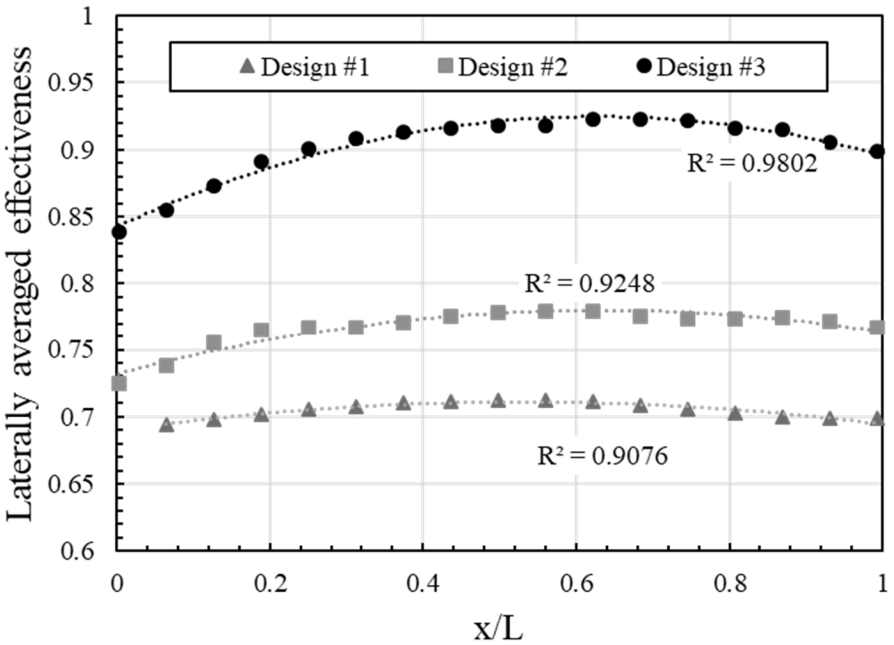

FIGURE 3.7 Laterally averaged effectiveness for Flow level 2. Dotted line is second order polynomial trend line for each data

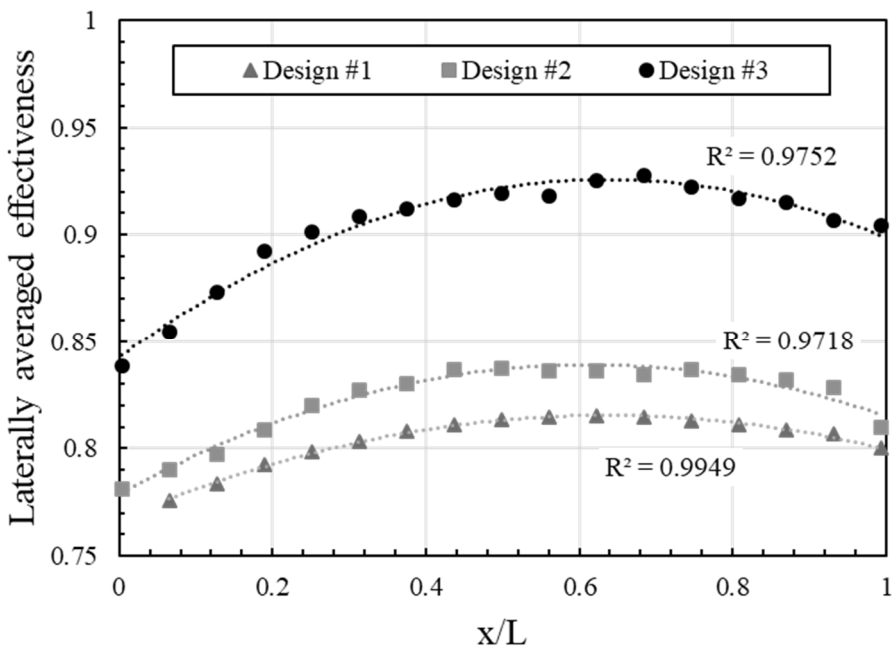

FIGURE 3.8 Laterally averaged effectiveness for Flow level 3. Dotted line is second order polynomial trend line for each data

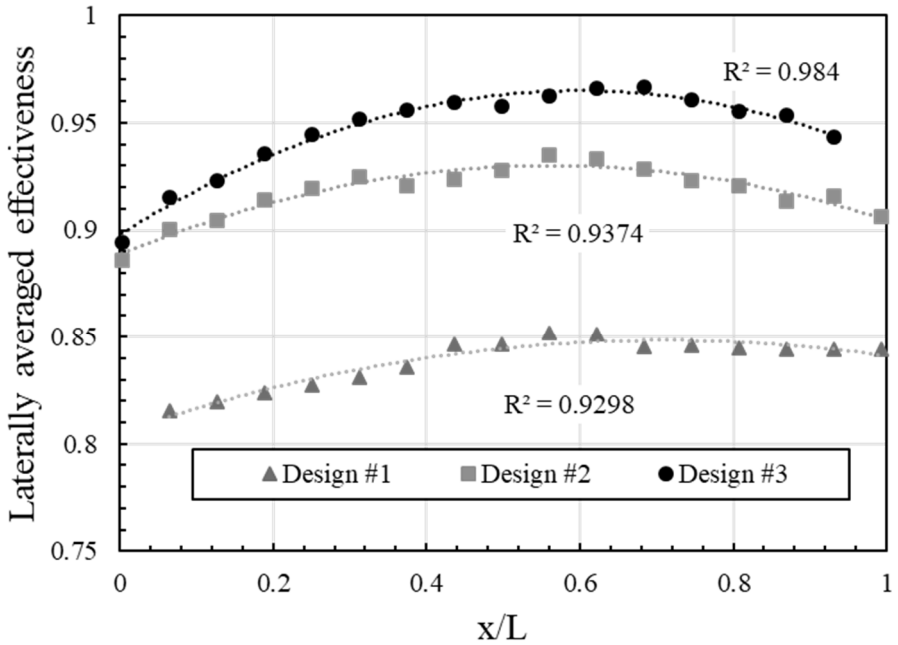

FIGURE 3.9 Laterally averaged effectiveness for Flow level 4. Dotted line is second order polynomial trend line for each data

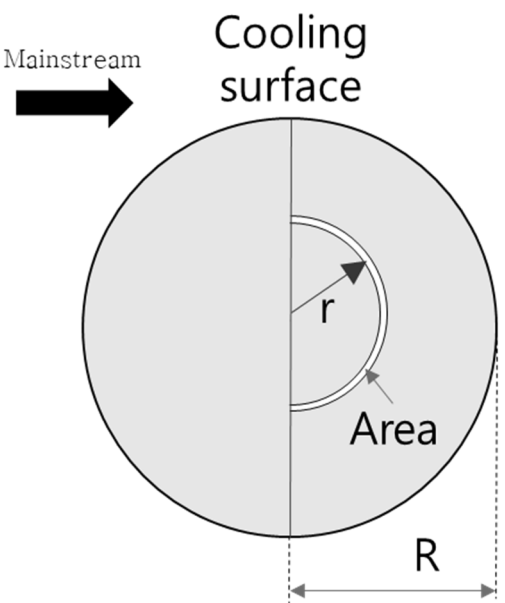

FIGURE 3.10 Schematic of half circle averaged effectiveness.

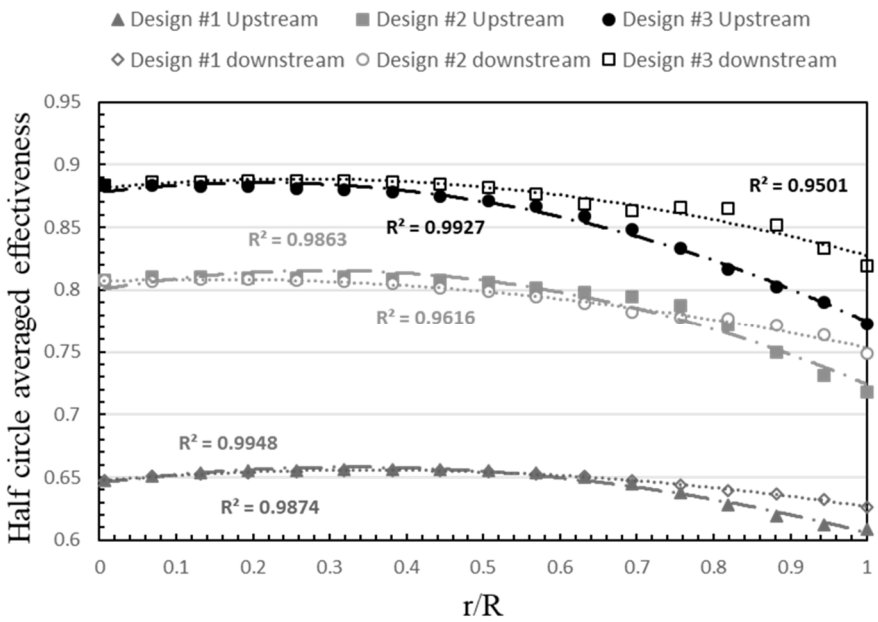

FIGURE 3.11 Half circle averaged effectiveness of flow level 1 case. Dotted line and dash dotted line are second order polynomial trend line for downstream and upstream, respectively

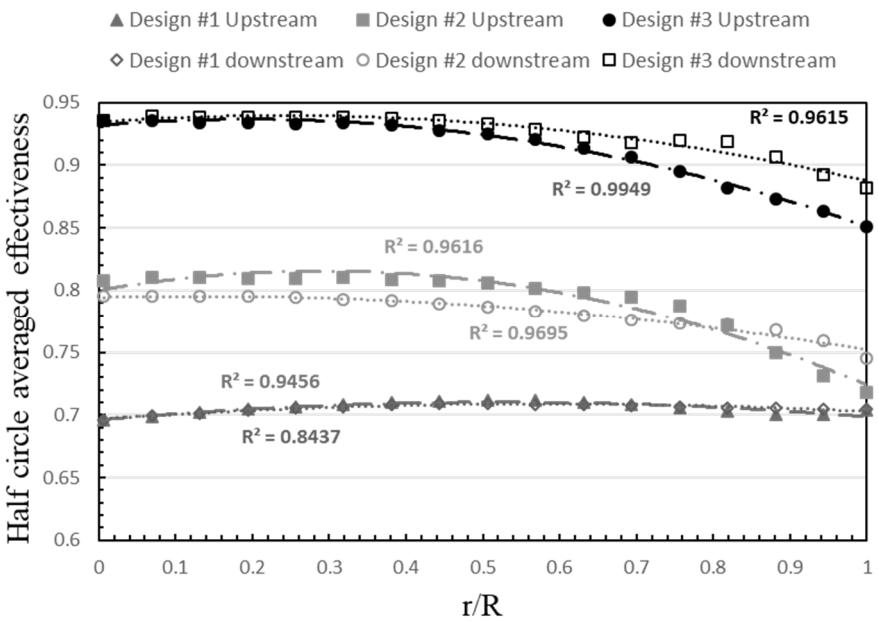

FIGURE 3.12 Half circle averaged effectiveness of flow level 2 case. Dotted line and dash dotted line are second order polynomial trend line for downstream and upstream, respectively

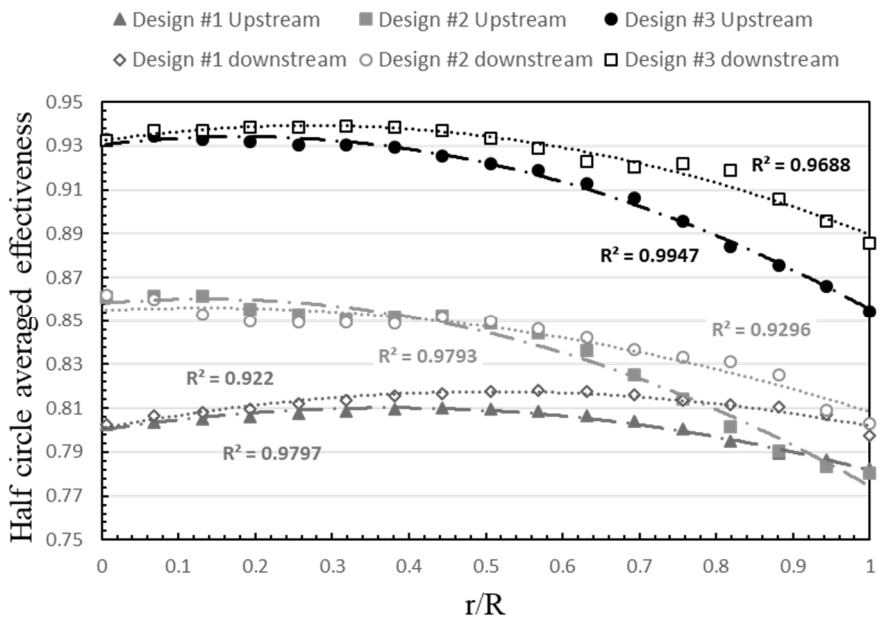

FIGURE 3.13 Half circle averaged effectiveness of flow level 3 case. Dotted line and dash dotted line are second order polynomial trend line for downstream and upstream, respectively

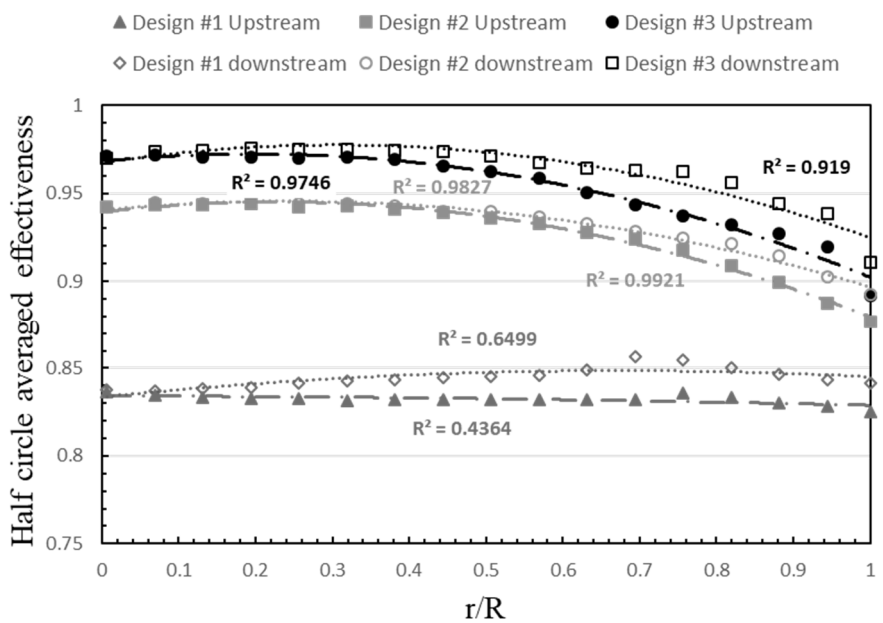

FIGURE 3.14 Half circle averaged effectiveness of flow level 4 case. Dotted line and dash dotted line are second order polynomial trend line for downstream and upstream, respectively

Chapter 4. Discussion

4.1. Computational Fluid Dynamics comparison

Fig. 4.1(a) shows the CFD effectiveness distribution for Design #3 at Flow Level 4, performed by fellow researcher Guwon Seon. Reynolds Averaged Navier-Stokes (RANS) with a commercial code, CFX, was used to solve this case. Compared with the experimental result, it shows the same trend where the downstream region near the center has the highest effectiveness, and upstream is less effective than downstream. However, the upstream edge has lower effectiveness and downstream edge has higher effectiveness compared to the experiments. Thus, the amount of mixing seems to be a bit different for RANS.

Figure 4.1(b) shows the flow structure in the x-y cross section. In this figure we can see how the coolant flow mixes with the main flow. The coolant flow from the upstream hole blows off, then reattaches on the cooling surface. The coolant flow from the downstream hole is just blown downstream by the main flow, and does not contribute to cooling of the surface. This corroborates the effectiveness distribution results from Chapter 3.1. Therefore, circular array film cooling is mainly due to the reattachment of the coolant flow coming from the upstream hole.

4.2. Sensitivity analysis

From the experimental results, we found that design #3 is the best, and the higher the flow rate, the better the cooling. From this, we can hypothesize that the larger the hole size and the greater the flow rate, the greater the effectiveness of the experiment. We conducted sensitivity analysis on the data to identify the key parameters.

A regression model was constructed with area averaged effectiveness as the Y factor. The initial X factors were # of hole, hole diameter, mass flow rate, and DR. The independence between these four factors was verified by multicollinearity evaluation. As a result of verifying the explanatory power of each factor including the square factor and interaction factor, factors excluding DR were used to construct the model. The equation for the model is Equation 4.1. R^2 is 0.9471. Y is area averaged effectiveness. X_1, X_2, and X_3 are mass flow rate, hole diameter and the number of holes, respectively.

$$Y = (-770 + 7.05X_1 + 1297\,X_2 + 93.8\,X_3 + 0.02\,X_1^2 - 1.78\,X_1 \times X_2) * 10^{-4} \cdots\cdots\cdots\cdots Equation\ 4.1$$

Based on the above model, we found that the hole diameter is the most sensitive parameter, and the number of holes is next. An increase in either parameter will greatly enhance the effectiveness.

However, a design with larger hole diameter or more holes than design #3 is not manufacturable. Thus, design #3 was downselected as the actual scaled-down purge tip to be used in the gas turbine monitoring application.

According to the sensitivity analysis, the maximum effectiveness is 0.9922 when the flow rate is maximum, the hole diameter is 6 mm, and the number of holes is 20. This coincides with our experimental result.

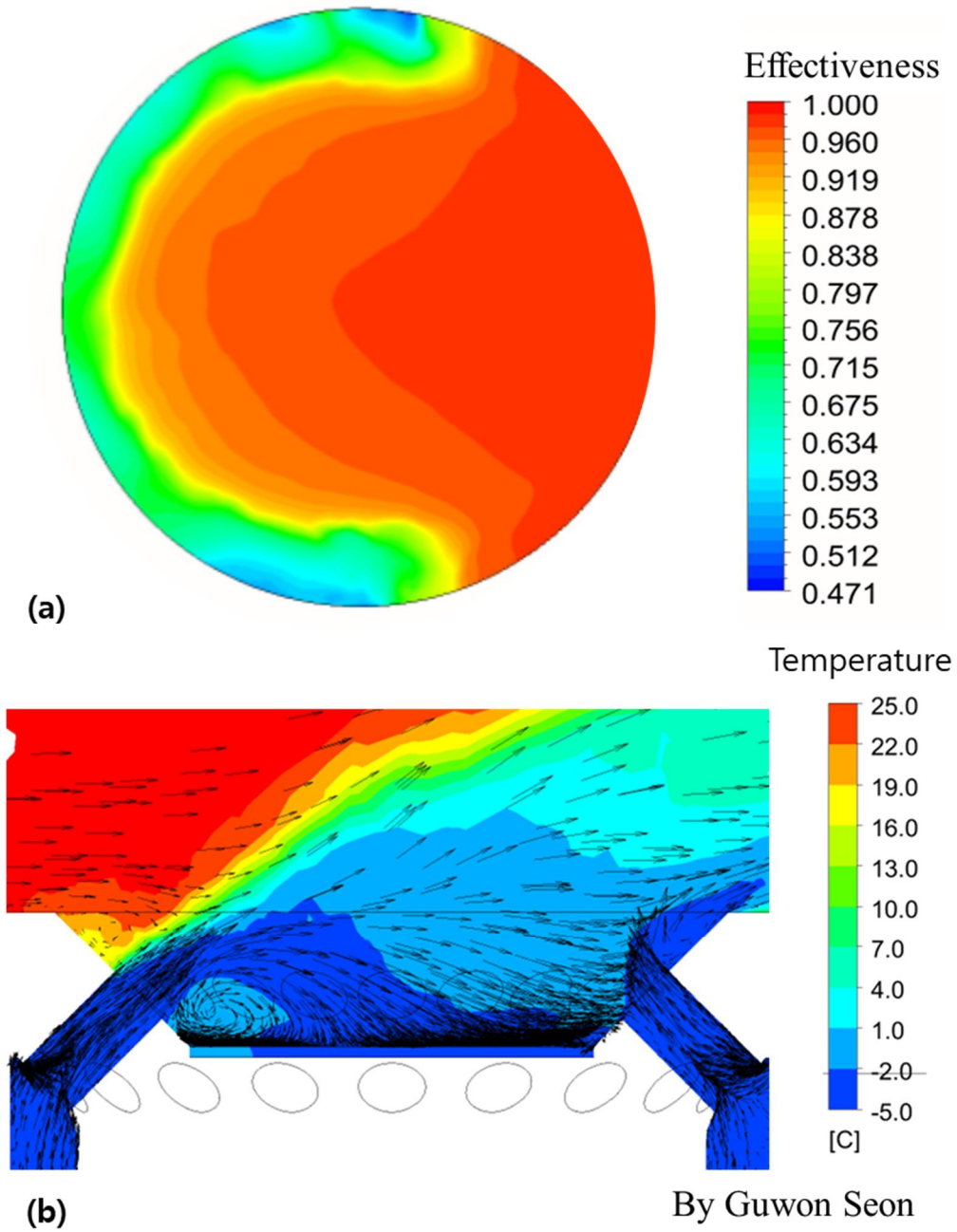

FIGURE 4.1 RANS CFD result for (a) top view and (b) side view. Contour represents effectiveness at (a). Vector represents velocity of each point and contour represents temperature at (b)

Chapter 5. Conclusion

In the present study, the effect of various parameters on circular array film cooling was investigated. The performance of circular array film cooling was generally lower at the outer edge, and lowest at the upstream region. Observation of the flow structure revealed that this is due to the coolant from the upstream hole blowing off and reattaching farther downstream, Downstream holes do not contribute much to the cooling. Additionally, we confirmed that the hole diameter is the most sensitive parameter.

In order to simplify the problem, we had to limit various factors. In the future, experiments should be performed using new parameters such as injection angle, surface angle, hole geometry, and downstream hole diameter. The velocity field of circular array film cooling should also be investigated through Particle Image Velocimetry (PIV), in order to validate the CFD results.

Bibliography

1. Bogard, D. and K. Thole, *Gas Turbine Film Cooling.* Journal of Propulsion and Power, 2006. **22**: p. 249-270.
2. Teekaram, A.J.H., C.J.P. Forth, and T.V. Jones, *The Use of Foreign Gas to Simulate the Effects of Density Ratios in Film Cooling.* Journal of Turbomachinery, 1989. **111**: p. 57-62.
3. Papell, S.S., *Effect on Gaseous Film Cooling of Coolant Injection Through Angled Slots and Normal Holes*. 1960.
4. Hartnett, J.P., R.C. Birkebak, and E.R.G. Eckert, *Velocity Distributions, Temperature Distributions, Effectiveness, and Heat Transfer for Air Injected Through a Tangential Slot into a Turbulent Boundary Layer.* Journal of Heat Transfer, 1961. **83**: p. 293-305.
5. Pedersen, D.R., E.R.G. Eckert, and R.J. Goldstein, *Film Cooling with Large Density Differences Between the Mainstream and the Secondary Fluid Mea- sured by the Heat-MassTransfer Analogy.* Journal of Heat Transfer, 1977. **99**: p. 620-627.
6. Baldauf, S., et al., *Correlation of Film-Cooling Effectiveness From Thermographic Measurements at Enginelike Conditions.* Journal of Turbomachinery, 2002. **124**(4): p. 686-698.
7. Baldauf, S., A. Schulz, and S. Wittig, *High resolution measurements of local effectiveness by discrete hole film cooling.* AMERICAN SOCIETY OF MECHANICAL ENGINEERS, 1999.
8. Thole, K.A., A.K. Sinha, and D.G. Bogard, *Mean temperature measurements of jets with a crossflow for gas turbine film cooling application*. Rotating Machinery Transport Phenomena, ed. J.H. Kim and W.J. Yang. 1992, New York: Hemisphere.
9. Sinha, a.K., D.G. Bogard, and M.E. Crawford, *Film-Cooling Effectiveness Downstream of a Single Row of Holes With Variable Density Ratio.* Journal of Turbomachinery, 1991. **113**: p. 442-449.
10. Saumweber, C., A. Schulz, and S. Wittig, *Free-Stream Turbulence Effects on Film Cooling with Shaped Holes.* ASME Turbo Expo, 2002: p. 41-49.
11. Schroeder, R.P. and K.A. Thole, *Thermal Field Measurements for a Shaped Hole at Low and High Freestream Turbulence Intensity.* 2016. **139**: p. 1-11.
12. Schmidt, D.L., B. Sen, and D.G. Bogard, *Film Cooling with Compound Angle Holes: Adiabatic Effectiveness.* Journal of Turbomachinery, 1996. **118**: p. 807-813.
13. Sen, B., D.G. Bogard, and D.L. Schmidt, *Film Cooling with Compound Angle Holes: Heat Transfer.* Journal of Turbomachinery, 1996. **118**: p. 800-806.
14. Saumweber, C. and A. Schulz, *Effects of Geometry Variations on the Cooling Performance of Fan-Shaped Cooling Holes.* Journal of Turbomachinery, 2012. **134**.

15. Ramesh, S., et al., *Film Cooling Performance of Tripod Antivortex Injection Holes Over the Pressure and Suction Surfaces of a Nozzle Guide Vane.* Journal of Thermal Science and Engineering Applications, 2017. **9**: .
16. Kohli, A. and D.G. Bogard, *Adiabatic Effectiveness, Thermal Fields,and Velocity Fields for Film Cooling with Large Angle Injection.* Journal of Turbomachinery, 1997. **119**: p. 352-358.
17. Foster, N.W. and D. Lampard, *The Flow and Film Cooling Effectiveness Following Injection Through a Row of Holes.* Journal of Engineering for Power, 1980. **102**: p. 584-588.
18. Han, J.-C. and A.B. Mehendale, *Flat-Plate Film Cooling with Steam Injection Through One Row and Two Rows of Inclined Holes.* Journal of Turbomachinery, 1986. **108**: p. 137-144.
19. Bashir, M.H., C.-C. Shiau, and J.-C. Han, *Film cooling effectiveness for three-row compound angle hole design onflat plate using PSP technique.* International Journal of Heat and Mass Transfer, 2017. **115**: p. 918-929.
20. Gao, Z. and J.-C. Han, *Influence of Film-Hole Shape and Angle on Showerhead Film Cooling Using PSP Technique.* Journal of Heat Transfer, 2009. **131**(061701): p. 11.
21. Roach, P.E., *The generation of nearly isotropic turbulence by means of grids.* International Journal of Heat and Fluid Flow, 1986. **8**(2): p. 11.
22. Boyd, E.J., et al., *Direct Measurement of Heat Transfer Coefficient Augmentation at Multiple Density Ratios.* Journal of Turbomachinery, 2017. **139**: p. 1-11.
23. Tropea, C., A. Yarin, and J.F. Foss, *Springer Handbook of Experimental Fluid Mechanics*. Vol. Vol.1. 2007, Berlin Heidelberg: Springer-Verlag
24. Vollmer, M. and K.-P. Mollmann, *Infrared thermal imaging: fundamentals, research and applications.* Second ed. 2017: John Wiley & Sons.
25. Bendat, J.S. and A. G.Piersol, *Random Data : Analysis and Measurement procedures*. Third ed. 2000: John Wiley & Sons.
26. Minkina, W. and S. Dudzik, *Infrared Themography : errors and uncertainties*. 2009: John Wiley & Sons.
27. Mouzon, B.D., et al., *Net Heat Flux Reduction and Overall Effectiveness for a Turbine Blade Leading Edge.* ASME Turbo Expo, 2005. **3**: p. 825-832.

환형 막냉각에 대한 실험적 분석

서울대학교 대학원
기계항공공학부
홍 준 영

요약

본 연구에서는 환형 막 냉각 기법의 유효도에 끼치는 여러가지 인자의 영향에 대해 실험적으로 분석하였다. 냉각 유효도는 적외선 카메라를 사용하여 측정된 온도를 무차원화하여 구해졌다. 실험은 시제품을 풍동에 장착하여 이루어졌으며 각 시제품은 서로 다른 개수와 지름의 구멍들이 환형으로 배열되어 있었다. 영역 평균 유효도는 유량과 함께 증가하였으며 6mm 지름의 구멍이 20개 있는 디자인이 가장 좋은 디자인으로 판명되었다. 각 인자들의 유효도에 대한 영향을 알아보기 위해 회귀분석이 수행되었고 구멍의 지름이 가장 영향이 큼을 알 수 있었다. 또한, 동료 연구자의 CFD로부터, 상류의 구멍에서 나온 유동이 표면 중앙의 하류부에 다시 접촉하고 하류의 구멍에서 나온 유동과 함께 주 유동으로 흘러감을 알 수 있었다.

주요어: 환형 막냉각, 적외선 카메라, 냉각 유효도
학번: 2017-27004